### MSEC2023-104454

## INHOUSE MULTI-MATERIAL NOZZLE SYSTEM DESIGN AND FABRICATION FOR 3D BIOPRINTING PROCESS: NEXT STEP

## Connor Quigley Department of Sustainable Product Design and Architecture, Keene State College, Keene, NH.

# Warren Hurd Department of Sustainable Product Design and Architecture, Keene State College, Keene, NH.

## Scott Clark Department of Sustainable Product Design and Architecture, Keene State College, Keene, NH.

## Rokeya Sarah Department of Sustainable Product Design and Architecture, Keene State College, Keene, NH.

## MD Ahasan Habib\* Department of Sustainable Product Design and Architecture, Keene State College, Keene, NH.

#### **ABSTRACT**

Three-dimensional (3D) bio-printing is a rapidly growing field attempting to recreate functional tissues for medical and pharmaceutical purposes. The printability of multiple materials encapsulating various living cells can take this emerging effort closer to tissue regeneration. In our earlier research, we designed a Y-like nozzle connector system capable of switching materials between more than one filament with continuous deposition. The device had a fixed switching angle, was made from plastic, and was suitable for one-time use. This paper presents the extension of our previously proposed nozzle system. We considered  $30^{\circ}$ ,  $45^{\circ}$ ,  $60^{\circ}$ , and  $90^{\circ}$  angles (vertical and tilted) between the two materials and chose stainless steel as a material to fabricate those nozzle connectors. The overall material switching time was recorded and compared to analyze the effects of those various angles. Our previously developed hybrid hydrogel (4% Alginate and 4% Carboxymethyl Cellulose, CMC) was used as a test material to flow through the nozzle system. These in-house fabricated nozzle connectors are reusable, easy to clean, and sterile, allowing smooth material transition and flow.

#### 1. INTRODUCTION

Three dimensional (3D) bioprinting technique is strongly recognized for fabricating patient-specific complex models with distinct biomaterials encapsulating living cells [1]. This technique is crawling towards to mimic tissue-specific microarchitecture closely as an emerging tool for tissue engineering. Among extrusion-, laser-, and ink jet-based 3D bioprinting technology, the first one allows for the deposit of various biomaterials enclosing a larger percentage of cells [2]. Natural hydrogels are good candidates to be bio-ink (biomaterial

encapsulated with living cells) due to their biocompatibility, less cytotoxicity, and high-water content (<90%) [3]. However, a few of them are typically used to prepare bio-ink because of their weak mechanical strength and crosslinking rate [4]. Successful interaction between various cells can expedite the tissue regeneration process [5]. Therefore, the capability to fabricate scaffolds with multiple materials encapsulating various type of cells can mimic the native tissue architecture and take the tissue regeneration effort one step further [6]. Various efforts have been reported to fabricate scaffolds with multiple materials. A multihead bioprinting technique has been reported to fabricate scaffolds with polycaprolactone (PCL) and alginate with chondrocytes and osteoblasts cells [7]. To demonstrate the ability to print heterogeneous and multi-functional hydrogel, multifunctional hydrogel structures, an effort was reported using varying chemical, electrical, mechanical, and biological properties by tuning process and material related parameters [8]. To incorporate elasticity and muscle development on one side and stiffness and tendon development on the other, polyurethane [9] with C2C12 cell and poly(ε-caprolactone) (PCL) with NIH/3T3 cell were printed using multi-head bioprinter [10]. Some other works have also been reported where multiple print heads have been used to fabricate multi-material scaffolds [11-

Recently we designed a nozzle system built with plastic, capable of switching materials between more than one filament with continuous deposition using an asymmetric Y-connector [15]. The device had a fixed switching angle [16], was made from plastic, and was suitable for one-time use. This paper presents an extension of our previously proposed nozzle system. We considered  $30^{0}$ ,  $45^{0}$ ,  $60^{0}$ , and  $90^{0}$  angles (vertical and tilted) between the two materials and chose stainless steel as a material to fabricate those asymmetric Y- nozzle connectors. The

proposed stainless-steel asymmetric Y-connector nozzle fits in to a 3D bioprinting system using connectors which are used with many printing systems and components such as plastic tips and 3ml syringes and check valves. To adjust with the existing resources such as 3D bioprinter, biomaterial used to extrude, and pressure source, our proposed nozzle can be easily customized and fabricated. The configuration of an asymmetric Y-connector was chosen for easier alignment with the existing bio-printers used. Certain existing designs use this asymmetric configuration which is made from Poly carbonate. The final material for our proposed connector is 304 and 316L stainless Steel that allows sanitization and reuse. The overall material switching time was recorded and compared to analyze the effects of those various angles. Our previously developed hybrid hydrogel (4% Alginate and 4% Carboxymethyl Cellulose, CMC) [17] was used as a test material to flow through the nozzle system. These in-house fabricated nozzle connectors are reusable, easy to clean, and sterile, allowing smooth material transition and flow.

#### 2. MATERIALS AND METHODS

### 2.1 Flow simulations though nozzle system

SolidWorks 3D Modeling and Flow Simulation Package (Dassault Systèmes SolidWorks Corporation, Waltham, MA) were used to model the nozzle connectors having  $30^{\circ}$ ,  $45^{\circ}$ ,  $60^{\circ}$ , and  $90^{\circ}$  angles (vertical and tilted) between the two material flows. For flow simulation, the viscosities of two materials published earlier such as 8% Alginate (A<sub>8</sub>) and 2% Alginate-6% Carboxymethyl Cellulose (A<sub>2</sub>C<sub>6</sub>) were used in this paper [15]. As an example, the detailed engineering drawing for a nozzle having 35-deg angle between two material flows is shown in Figure 1.

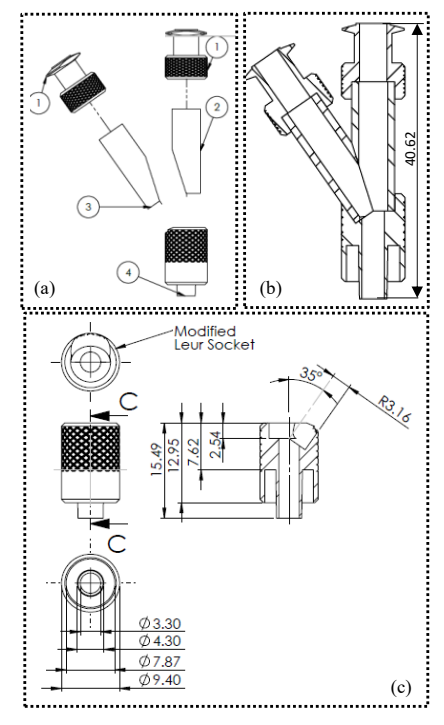


**Figure 1:** (a) EXPLODED VIEW OF A NOZZLE, (b) CROSS-SECTIONAL VIEW OF THE MODELED NOZZLE, AND (c) DIMENSIONS FOR OUTLET NOZZLE HOLDER.

Various extrusion pressures such as 100 kPa, 150 kPa, and 200 kPa and viscosities equivalent to two material compositions such as  $A_2C_6$  and  $A_8C_0$  were used to simulate the flow through the nozzles. Pressure distribution at the intersection of two materials was recorded as an output.

## 2.2 Preparation of 3D bioprinter and related process parameters

A three-axis multi-head (three-extruders) BioX (CELLINK, Boston, MA) 3D bioprinter was used to extrude hydrogels. Material transition time i.e., time required to change the material flow from one type (100% M<sub>1</sub>) to another type (100% M<sub>2</sub>) in the coaxial nozzle systems was determined as shown in Figure 2(c). Material from one nozzle was fully extruded into the empty nozzle connector until it had reached the tip. The material from the other nozzle was then extruded continuously until it was visibly extruded at the nozzle tip. Time required of the 2 angles (axial and tilted nozzle) was recorded and analyzed to see how the angle variation affects the material transition. Our previously developed hybrid hydrogel (4% Alginate and 4% CMC;  $A_4C_4$ ) [17] was used as a test material to flow through the nozzle system. An extrusion pressure of 110 kPa was applied.

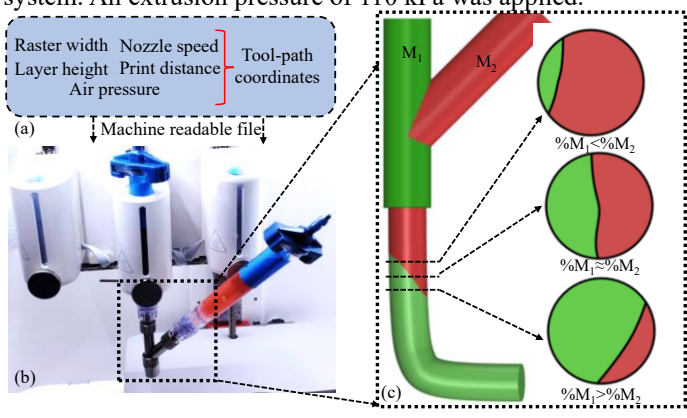


**Figure 2:** (a) 3D PRINTING PROCESS PARAMETERS USED TO PREPARE MACHINE-READABLE FILE, (b) ATTACHING NOZZLE CONNECTOR TO 3D PRINTER HEAD, AND (c) AN SCHEMATIC OF MATERIAL DISTRIBUTION WITH CROSS-SECTION AT THREE LOCATIONS.

To fabricate the scaffolds extruding through nozzle connectors having  $30^{\circ}$ ,  $45^{\circ}$ ,  $60^{\circ}$ , and  $90^{\circ}$  angles, the prepared  $A_4C_4$  hybrid hydrogel was stored in two disposal syringes and extruded pneumatically following a layer-upon-layer fashion through a nozzle having 410  $\mu$ m diameter on a stationary build plane. Various printing parameters such as nozzle diameter, air pressure, nozzle speed, and print distance (i.e., the perpendicular distance between the nozzle tip and print bed) can control the deposition rate of the material [18]. The print speed and print distance used in fabricating the scaffold were 10 mm/s and 0.405mm respectively.

A computer-aided design (CAD) software, Rhino 6.0 (https://www.rhino3d.com), was used to design and define the vectorized toolpath of a scaffold. Slicer (https://www.slicer.org), a G-code generator software is used to generate a Bio-X compatible file including the toolpath coordinates and all process parameters to fabricate the scaffold. fabricated scaffold after the print. Two syringes of A<sub>4</sub>C<sub>4</sub> were prepared and dyed with either red or blue food coloring. They were loaded onto the printer and the 45-degree nozzle was attached to both syringes with check valves between the nozzle and syringes. A 0.41mm plastic tapered syringe tip was used for printing. Each syringe was pressurized initially to fill in the empty space of the nozzle they were pressurized until only one material was coming out of the plastic tip. The model used to print was a prismatic box 20mm x 20mm x 1mm, the layer height was set to 0.3mm, and an infill percent of 11% was used. The print pressure was set to 130 kPa, and the print speed was set to 7.0 mm/s. The layer height, applied pressure, and print speed were optimized in our earlier work [17, 19]. The print was recorded to examine the color-changing and mixing behavior. The overall scaffold fabrication process is schematically shown in Figure 2.

## 2.3 Fabrication of nozzle system: 3D printing and metallic

After modeling all nozzle connectors using SolidWorks 3D Modeling software, we printed them using a Raised 3D printer (Irvine, CA) as shown in Figure 3. The internal and external diameter of the nozzle connector were 5.35mm and 6.35mm respectively. Total length from the tip of the tapered nozzle to the end is 144 mm where the length of tapered nozzle is 24 mm as shown in Figure 9(b). Nozzle connectors were fabricated using stainless steel because the material being used will potentially be composed of live cell cultures. The intent is to sterilize the fittings between tests so the fittings can be reused.

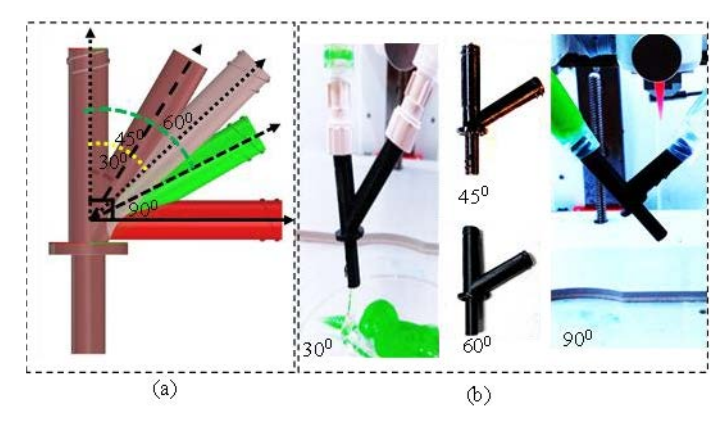


**Figure 3:** (a) 3D MODEL FOR VARIOUS NOZZLE CONNECTORS AND (b) 3D PRINTED NOZZLES.

303 stainless steel Luer fittings and 304 Stainless steel tubing was purchased from McMaster-Carr McMaster-Carr (Elmhurst, IL). The fittings were modified in house with the Bridgeport machine to fit onto the 304 stainless steel tubing. Previous plastic prototype fitting had an OD of 0.249 and an ID

of 0.152". The tubing for four connectors had an OD of 0.249 and an ID of 0.169. Tubing was initially cut with a small horizontal bandsaw (General International: Model BS5205, Whitehouse, OH) to a length of 0.8". The ends were then milled perpendicular on a Bridgeport Milling Machine (Atlanta, GA) fitted with a quick release C5 Collet fixture to hold the tubing. A device with a three-jaw chuck was mounted on a separate Bridgeport machine to set different angles. The device was used to mill one half the desired angle on each tube. The angle was on one end of the tube and went to half of the diameter of the tube. There was a pair of tubes for each part. The exception was the ninety-degree fitting. That cut was not made at the end of the tube for ease of manufacturing. After the cut was made the threejaw chuck would be rotated 180° and a relief cut using a 0.1562 diameter cutter was made on one part of the pair to provide clearance for the flow.

Parts were hand assembled and welded with a Coherent Rofin StarWelder (Baasel Lasertech, Gilching, Germany). Single laser pulses were applied with a foot pedal while the parts were held under a microscope. Each individual pulse was applied for 5 milliseconds with an average power of 2.3 kW and 0.3mm diameter. The pulse shape is divided into five segments with power settings of 80% 100% 90% 75% 50% respectively. Pulse overlap was between 50% & 75%. All external seams were welded. Some stainless steel 304 filler wire was added to fill any voids. The 304 stainless in the tubing was easier to weld because of the lower sulfur content. Parts were cleaned with a small wire brush and returned to their respective baggies. The overall nozzle manufacturing steps are shown in Figure 4.

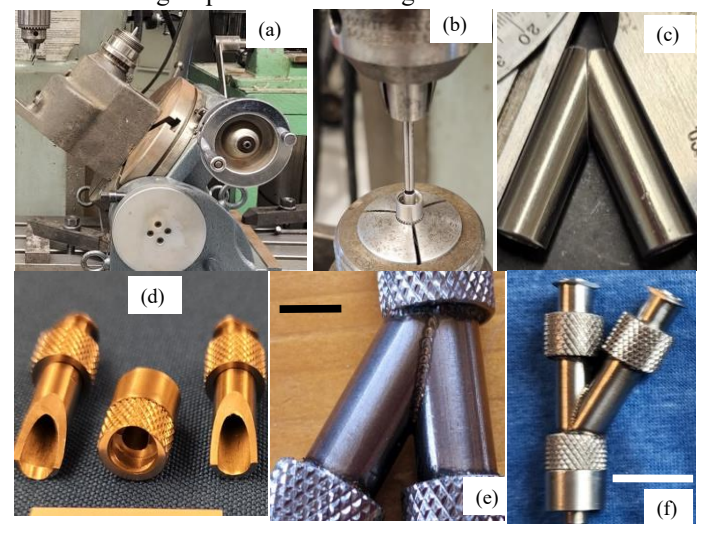


**Figure 4:** (a) THREE-JAW CHUCK TO SET DIFFERENT ANGLES, (b) MILLING FOR A SPECIFIC ANGLES, (c) MILLED PARTS FOR A SPECIFIC ANGLE, (d) THREE PARTS READY TO WELD (SCALE BAR 6 mm), AND (e) LASER WELDED PARTS, (f) FINAL PART (SCALE BAR 28 mm).

### 3. RESULTS AND DISCUSSION

### 3.1 Flow simulations for various nozzle connectors

All simulation results for  $A_2C_6$  and  $A_4C_4$  are shown in Figure (5-8) for  $30^0$ ,  $45^0$ ,  $60^0$ , and  $90^0$  respectively. In the simulations, the fluid would briefly enter the angled connector piece before flowing back down. This could be considered backflow, but the simulations did not show the degree of backflow that the nozzles experienced. The simulations also didn't show backflow traveling up the straight part of the nozzles. Every nozzle tested had some degree of backflow, so none of the designs were able to negate that on their own, but the problem was easily fixed by using check valves.

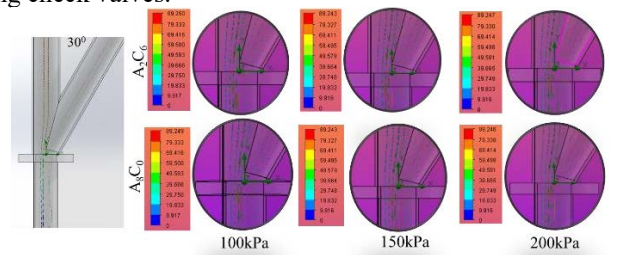


**Figure 5:** FLOW SIMULATION OF THE NOZZLE CONNECTOR HAVING 30° ORIENTATIONS WITH TWO MATERIALS FLOW.

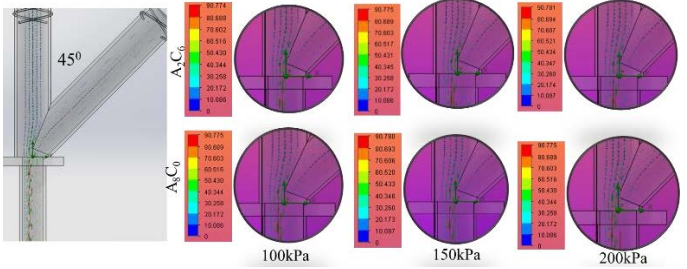


**Figure 6:** FLOW SIMULATION OF THE NOZZLE CONNECTOR HAVING 45° ORIENTATIONS WITH TWO MATERIALS FLOW.

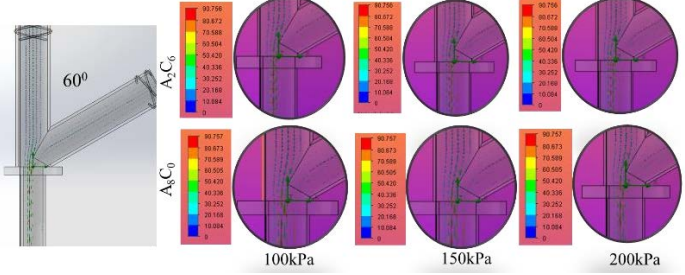


**Figure 7:** FLOW SIMULATION OF THE NOZZLE CONNECTOR HAVING 60<sup>0</sup> ORIENTATIONS WITH TWO MATERIALS FLOW.

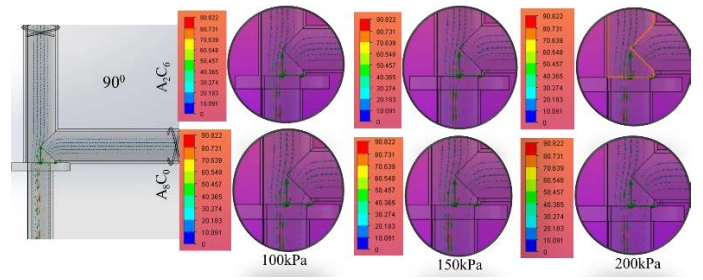


**Figure 8:** FLOW SIMULATION OF THE NOZZLE CONNECTOR HAVING 90° ORIENTATIONS WITH TWO MATERIALS FLOW.

Flow simulations for 30°nozzle connector was conducted for three different applied pressures such as 181325, 201325, and 221325 Pa from nozzle tip to the end point of the arrangement. From the shear rate distribution for each nozzle connector, it is clear that higher applied pressure showed larger shear rate at the tip. Figure 9(a) shows shear stress distribution for 201325 Pa applied pressure where a small backflow was observed. None of the designs were able to negate backflow on their own, but the problem was easily fixed by using check valves. Figure 9(b) shows overall shear strain distribution for three applied pressures of 181325, 201325, and 221325 Pa from nozzle tip to 73.47 mm. The simulation result shows 50% and 20% higher shear rate for 22% and 10% increment of applied pressure compared to the applied pressure of 181325 Pa. Similar characteristics were resulted in for 45°, and 90° nozzle connectors.

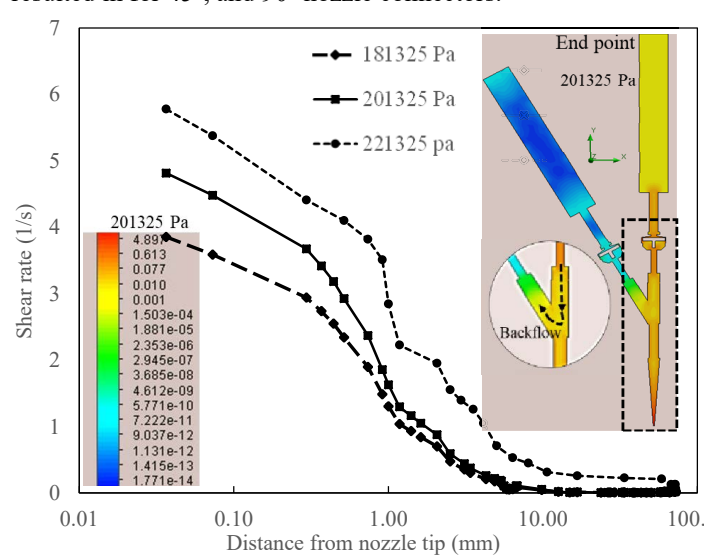


**Figure 9:** (a) DISTRIBUTION OF SHEAR RATE IN 30<sup>o</sup> NOZZLE CONNECTORS FOR 201325 PA APPLIED PRESSURE AND (b) DISTRIBUTION OF SHEAR RATE FOR THREE APPLIED PRESSURES OF 181325, 201325, AND 221325 PA FROM NOZZLE TIP TO 73.47 MM.

## 3.2 Fabricated metal nozzle connectors and materials flow through them

Following the methods described in section 2.3, we fabricated total four nozzle connectors having  $30^{\circ}$ ,  $45^{\circ}$ ,  $60^{\circ}$ , and  $90^{\circ}$  angles as shown in Figure 10 (b). All connectors were used to determine the material transition time from one material ( $M_1$ ) to another ( $M_2$ ) as shown in Figure 12 and 13. Material from one nozzle was fully extruded into the empty nozzle connector until it has reached the tip. Time required for this operation is defined as "axial delay" time. The material from the other nozzle was extruded continuously until it is visibly extruded at the nozzle tip. Time needed for this operation is defined as "tilted delay" time. The summation of "axial delay" and "tilted delay" is termed as the "total time". Nozzle connector having  $30^{\circ}$  showed highest axial time where  $90^{\circ}$  showed the lowest.

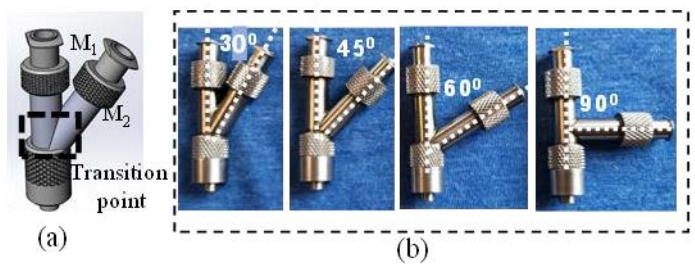


**Figure 10:** (a) 3D MODEL FOR A 30<sup>0</sup> NOZZLE CONNECTOR REPRESENTING TWO MATERIAL CONNECTION AND TRANSITION POINT. (b) NOZZLE CONNECTORS HAVING 30<sup>0</sup>, 45<sup>0</sup>, 60<sup>0</sup>, AND 90<sup>0</sup> ANGLE BETWEEN TWO MATERIAL FLOWS.

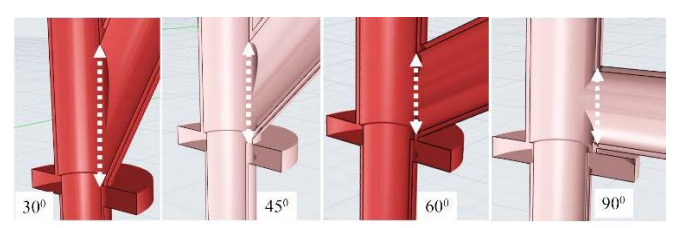


**Figure 11:** DIFFERENCE OF OPENING LENGTH THROUGH CONNECTORS HAVING (a) 30° ANGLE AND (b) 45° ANGLE FOR MATERIAL TRANSITION FROM ONE TYPE TO ANOTHER.

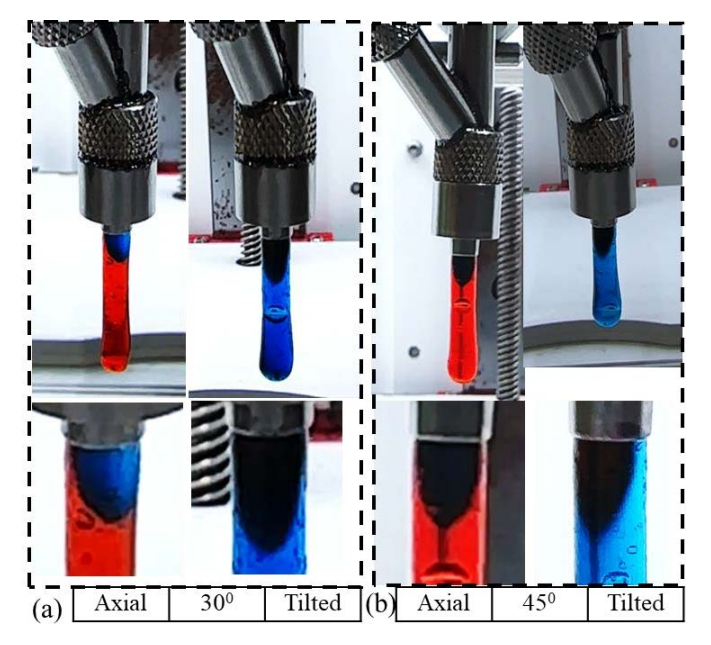


**Figure 12:** MATERIAL TRANSITION FROM AXIAL TO TILTED NOZZLE THROUGH CONNECTORS HAVING (a) 30° ANGLE AND (b) 45° ANGLE.

The possible reason is the intersection length of axial and tilted connectors of nozzles having 30°, 45°, and 60° are 100%, 41%, and 15.5% larger respectively compared to nozzle having 90° as shown in Figure 11. Even we used check valve to reduce the backflow of material during extrusion through axial

connector, higher intersection length may allow material entry to tilted connector. In case of tilted connector, nozzle having  $45^{\rm 0}$  and  $90^{\rm 0}$  showed lowest titled delay time where  $60^{\rm 0}$  showed the highest. For both  $45^{\rm 0}$  and  $90^{\rm 0}$ , material  $M_1$  showed minimal entry to tilted nozzle during axial flow resulting quickest flow of material  $M_2$ . Therefore, nozzle connector having angles  $45^{\rm 0}$  and  $90^{\rm 0}$  showed the lowest total time to shift from material  $M_1$  to

material M<sub>2</sub> as shown in Figure 14.

(a) Axial 60° Tilted (b) Axial 90° Tilted

**Figure 13:** MATERIAL TRANSITION FROM AXIAL TO TILTED NOZZLE THROUGH CONNECTORS HAVING (a) 60° ANGLE AND (b) 90° ANGLE.

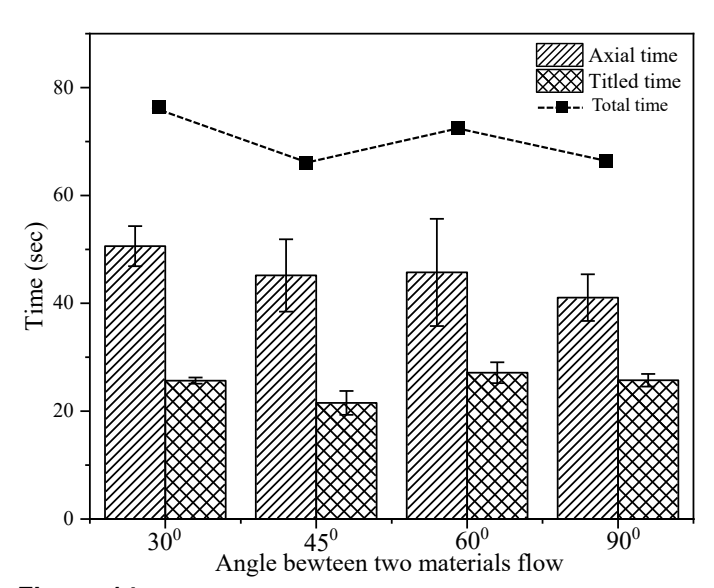


**Figure 14:** TIME REQUIRED TO FLOW FROM ONE TYPE OF MATERIAL TO ANOTHER TYPE. TOTAL TIME REPRESENTS CHANGING FROM PURELY ONE TYPE MATERIAL TO ANOTHER TYPE OF MATERIAL.

## 3.3 Material distribution through metallic nozzle connectors

To analyze the distribution of material during flow through the nozzle connector closely, we used the connector without a plastic tip. A set of filaments were fabricated using all nozzle connectors having angles of 30°, 45°, 60°, and 90°. As an example, a filament fabrication process using 300 nozzle connector is shown in Figure 14(a). The material distribution throughout the filament was analyzed following a technique shown in Figure 15 (b-c). The fabricated filament was crosslinked with CaCl<sub>2</sub> for 5-7 minutes and sliced to get the cross sections at different locations of filament to analyze the material distribution as shown Figure 15 (b). Even the fabricated filament was close to circular in shape after crosslinking, during slicing the filament failed to maintain the similar shape. Cross section of filaments fabricated by all nozzle connectors are shown in Figure 15 where all of them showed material distribution at various level. Rhino and ImageJ software were used to process the images of those cross sections to analyze the material distribution.

From the cross-sectional view of each filament (Figure 16) and material distribution calculation (Figure 17), we observed that filament extruded through the nozzle connectors having angles of  $30^{0}$  and  $45^{0}$  showed smooth material transition.

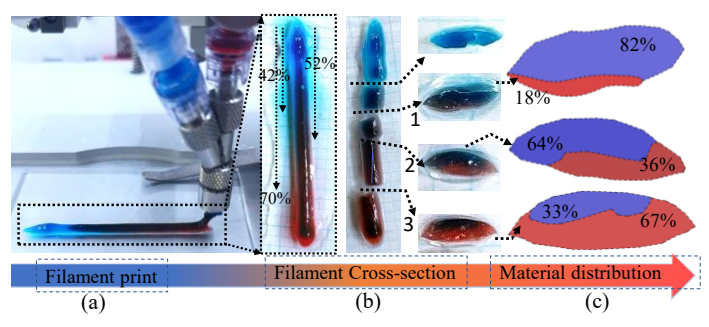


**Figure 15:** (a) FABRICATING FILAMENT WITH NOZZLE CONNECTOR HAVING 30° ANGLE, (b) SLICING TO EXTRACT THE CROSS-SECTION OF FILAMENT AT DIFFERENT LOCATIONS (START, MIDDLE, AND END), AND (c) MATERIAL DISTRIBUTIONS AT DIFFERENT LOCATIONS SUCH AS 42% (LOCATION 1), 52% (LOCATION 2), AND 70% (LOCATION 2) AWAY FROM THE TOP END OF THE FILAMENT WHERE IT SHOWS MATERIAL 1 CHANGES FROM 82% TO 33%.

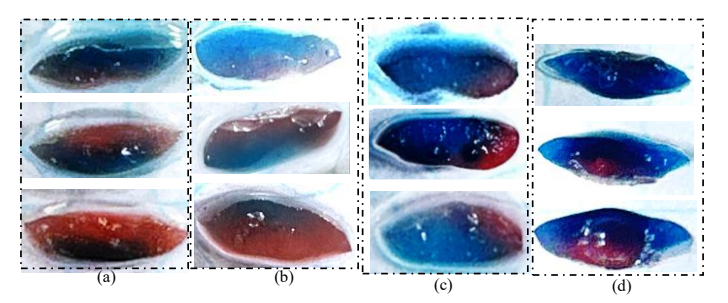


**Figure 16:** MATERAL DISTRIBUTION INTO THE FILAMENT AT DIFFERENT LOCATIONS FABRICATED WITH NOZZLE CONNECTOS (a) 30°, (b) 45°, (c) 60°, AND (d) 90°.

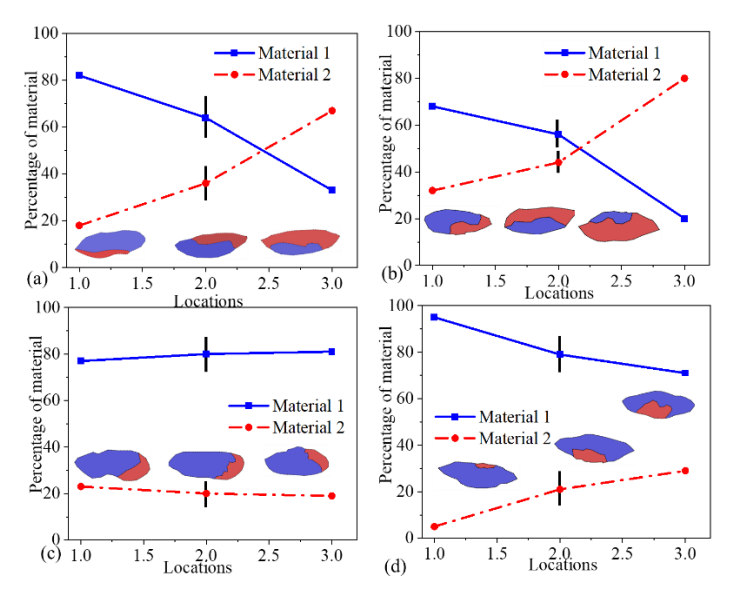


**Figure 17:** MATERAL DISTRIBUTION INTO THE FILAMENT AT DIFFERENT LOCATIONS FABRICATED WITH NOZZLE CONNECTOS (a) 30°, (b) 45°, (c) 60°, AND (d) 90°. TO TEST THE REPEATABILITY, THE CROSS SECTION AT LOCATION 2 WERE TAKEN THREE TIMES AND IT DID NOT SHOW THE SIGNIFICANT DIFFERENCE.

## 3.4 Scaffolds fabricated through needle connected to the metallic nozzle connector

Finally, we fabricated scaffolds with a 45-degree nozzle connector. Two syringes of  $A_4C_4$  were prepared and dyed with either red or blue food coloring. They were loaded onto the printer and the 45-degree nozzle was attached to both syringes with check valves between the nozzle and syringes. First of all, red colored material was extruded for the first layer followed by the blue colored material. From the flow diagram of Figure 18(a) to Figure 18(f), the material shifting of material from red color to blue was clearly visible.

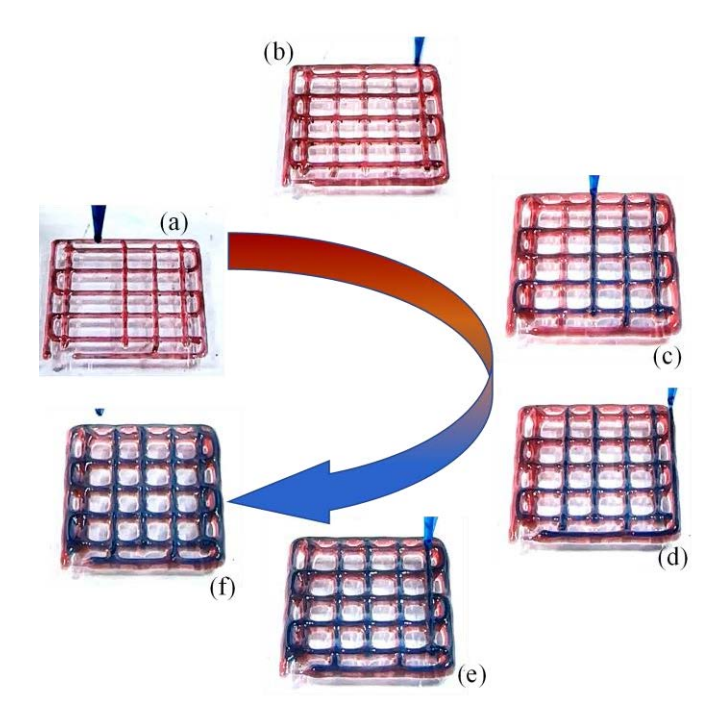


**Figure 18:** MATERIAL DISTRIBUTION THROUGHOUT THE PRINTING PROCESS FROM MATERIAL 1 TO MATERIAL 2. BLUE MATERIAL DISTRIBUTION AT (a) T=1 SEC, (b) T=15 SEC, (c) T=56 SEC, (d) T=98 SEC, (e) T=101 SEC, and (f) T=138 SEC. THREE TIMES PRINTED AND SIMILAR DISTRIBUTION OBSERVED.

#### 4. CONCLUSION

As an extension of our previous work, we considered 30°, 45°, 60°, and 90° angles (vertical and tilted) between the two materials and chose stainless steel as a material to fabricate nozzle connectors. We determined and compared the overall material switching time to analyze the effects of those various angles. Our previously developed hybrid hydrogel (4% Alginate and 4% Carboxymethyl Cellulose, CMC) was used as a test material to flow through the nozzle system. We observed closely the material distribution into the filament during the extrusion through nozzle connector and nozzle itself. In future, we will identify the material transition time during extrusion through the nozzle connecting it to all nozzle connectors. We will also identify the effect of material viscosity (using material composition other than A<sub>4</sub>C<sub>4</sub>) on the material transition for all connectors and nozzle connected to the connector. Finally, our long-term goal is using those nozzle connectors to extrude multiple materials encapsulating living cells.

#### **ACKNOWLEDGEMENTS**

Research was supported by New Hampshire-EPSCoR through BioMade Award #1757371 from National Science Foundation and New Hampshire-INBRE through an Institutional Development Award (IDeA), P20GM103506, from the National Institute of General Medical Sciences of the NIH.

#### Reference

- [1] S. V. Murphy and A. Atala, "3D bioprinting of tissues and organs," *Nature biotechnology*, vol. 32, no. 8, pp. 773-785, 2014.
- [2] H.-J. Kong, K. Y. Lee, and D. J. Mooney, "Decoupling the dependence of rheological/mechanical properties of hydrogels from solids concentration," *Polymer*, vol. 43, no. 23, pp. 6239-6246, 2002.
- [3] K. Markstedt, A. Mantas, I. Tournier, H. c. Martinez Ávila, D. Hagg, and P. Gatenholm, "3D bioprinting human chondrocytes with nanocellulose–alginate bioink for cartilage tissue engineering applications," *Biomacromolecules*, vol. 16, no. 5, pp. 1489-1496, 2015.
- [4] Y. He *et al.*, "Characterization and application of carboxymethyl chitosan-based bioink in cartilage tissue engineering," *Journal of Nanomaterials*, vol. 2020, 2020.
- [5] D. Howard, L. D. Buttery, K. M. Shakesheff, and S. J. Roberts, "Tissue engineering: strategies, stem cells and scaffolds," *Journal of anatomy*, vol. 213, no. 1, pp. 66-72, 2008.
- [6] D. B. Kolesky, K. A. Homan, M. A. Skylar-Scott, and J. A. Lewis, "Three-dimensional bioprinting of thick vascularized tissues," *Proceedings of the National Academy of Sciences*, vol. 113, no. 12, pp. 3179-3184, 2016.
- [7] J.-H. Shim, J.-S. Lee, J. Y. Kim, and D.-W. Cho, "Bioprinting of a mechanically enhanced three-dimensional dual cell-laden construct for osteochondral tissue engineering using a multi-head tissue/organ building system," *Journal of Micromechanics and Microengineering*, vol. 22, no. 8, p. 085014, 2012.
- [8] T. Xu *et al.*, "Hybrid printing of mechanically and biologically improved constructs for cartilage tissue engineering applications," *Biofabrication*, vol. 5, no. 1, p. 015001, 2012.
- [9] K. Hixon, C. Eberlin, P. Kadakia, S. McBride-Gagyi, E. Jain, and S. Sell, "A comparison of cryogel scaffolds to identify an appropriate structure for promoting bone regeneration," *Biomedical Physics & Engineering Express*, vol. 2, no. 3, p. 035014, 2016.
- [10] T. K. Merceron *et al.*, "A 3D bioprinted complex structure for engineering the muscle–tendon unit," *Biofabrication*, vol. 7, no. 3, p. 035003, 2015.
- [11] J. Kundu, J. H. Shim, J. Jang, S. W. Kim, and D. W. Cho, "An additive manufacturing-based PCL-alginate-chondrocyte bioprinted scaffold for cartilage tissue engineering," *Journal of tissue engineering and regenerative medicine*, vol. 9, no. 11, pp. 1286-1297, 2015.
- [12] A. K. Miri *et al.*, "Microfluidics-enabled multimaterial maskless stereolithographic bioprinting," *Advanced Materials*, vol. 30, no. 27, p. 1800242, 2018.

- [13] S. Sakai, K. Ueda, E. Gantumur, M. Taya, and M. Nakamura, "Drop-On-Drop Multimaterial 3D Bioprinting Realized by Peroxidase-Mediated Cross-Linking," *Macromolecular rapid communications*, vol. 39, no. 3, p. 1700534, 2018.
- [14] L. Ruiz-Cantu, A. Gleadall, C. Faris, J. Segal, K. Shakesheff, and J. Yang, "Multi-material 3D bioprinting of porous constructs for cartilage regeneration," *Materials Science and Engineering: C*, vol. 109, p. 110578, 2020.
- [15] C. Nelson, S. Tuladhar, and M. A. Habib, "Designing an Interchangeable Multi-Material Nozzle System for 3D Bioprinting Process," in *International Manufacturing Science and Engineering Conference*, 2021, vol. 85062: American Society of Mechanical Engineers, p. V001T03A005.
- [16] E. C. Novosel, C. Kleinhans, and P. J. Kluger, "Vascularization is the key challenge in tissue engineering," *Advanced drug delivery reviews*, vol. 63, no. 4, pp. 300-311, 2011.
- [17] A. Habib, V. Sathish, S. Mallik, and B. Khoda, "3D printability of alginate-carboxymethyl cellulose hydrogel," *Materials*, vol. 11, no. 3, p. 454, 2018.
- [18] H. Wang, S. Vijayavenkataraman, Y. Wu, Z. Shu, J. Sun, and J. Y. H. Fuh, "Investigation of process parameters of electrohydro-dynamic jetting for 3D printed PCL fibrous scaffolds with complex geometries," *International Journal of Bioprinting*, vol. 2, no. 1, pp. 63-71, 2016.
- [19] C. Nelson, S. Tuladhar, L. Launen, and M. Habib, "3D Bio-Printability of Hybrid Pre-Crosslinked Hydrogels," *International Journal of Molecular Sciences*, vol. 22, no. 24, p. 13481, 2021.